

# Ion-Induced Surface Diffusion in Ion Sputtering

Maxim A. Makeev and Albert-László Barabási

*Department of Physics, University of Notre Dame, Notre Dame, IN 46556*

(January 13, 2022)

Ion bombardment is known to enhance surface diffusion and affect the surface morphology. To quantify this phenomenon we calculate the ion-induced diffusion constant and its dependence on the ion energy, flux and angle of incidence. We find that ion bombardment can both enhance and suppress diffusion and that the sign of the diffusion constant depends on the experimental parameters. The effect of ion-induced diffusion on ripple formation and roughening of ion-sputtered surfaces is discussed and summarized in a morphological phase diagram.

PACS numbers: 79.20.Rf, 64.60.Ht, 68.35.Rh

Sputtering, the removal of atoms from the surface of solids through the impact of energetic particles (ions), is an important thin film processing technique [1]. Consequently, much attention has been focused on the measurement and calculation of the sputtering yield and of the velocity and angular distribution of the sputtered particles. However, for many applications an equally important phenomenon, ion-induced surface diffusion, has eluded sufficient understanding so far. In the absence of ion bombardment surface diffusion is thermally activated and characterized by the diffusion constant  $D_T = D_0 \exp[-E_d/k_B T]$  such that the evolution of the surface height  $h(x, y, t)$  is described by the continuum equation  $\partial h / \partial t = -D_T \nabla^4 h$  [2]. Here  $E_d$  is the activation energy for surface diffusion of the adatoms and  $T$  is the substrate temperature. However, numerous experiments investigated the effect of ion bombardment on island formation, surface migration, surface smoothing and ripple formation have provided evidence that ion bombardment is accompanied by an increase in surface diffusion [3–8]. In particular, it has been demonstrated that ion-induced surface diffusion can decrease the epitaxial temperature [3], enhance nucleation during growth [4], or modify the surface morphology. For example, MacLaren *et al.* [5] bombarded GaAs with 17 KeV  $\text{Cs}^+$  in the temperature range from  $-50$  to  $200^\circ\text{C}$ , observing the development of a ripple structure on the surface with a wavelength proportional to the square root of the diffusion constant. When decreasing the temperature, the ripple spacing (wavelength) did not decrease exponentially to zero with the inverse temperature, but at approximately  $60^\circ\text{C}$  it stabilized at a constant value, providing direct evidence for a temperature independent ion-induced surface diffusion constant.

Although the effect of the ions on surface diffusion is well documented experimentally, there is no theory that would quantify it. In this paper we calculate analytically the ion-induced diffusion constant,  $D^I$ , and its dependence on the ion energy, flux, angle of incidence, and penetration depth. We find that there exists a parameter range when ion bombardment generates a *negative* surface diffusion constant, leading to morphological instabilities along the surface, affecting the surface rough-

ness and the ripple structure. The effect of ion-induced diffusion on the morphology of ion-sputtered surfaces is summarized in a morphological phase diagram, allowing for direct experimental verification of our predictions.

Ion-sputtering is determined by atomic processes taking place within a finite penetration depth inside the bombarded material. The ions penetrate the surface and transfer their kinetic energy to the atoms of the substrate by inducing cascades of collisions among the substrate atoms, or through other processes, such as electronic excitations. A convenient picture of the ion bombardment process is shown in Fig. 1. The ions penetrate a distance  $a$  inside the solid before they completely spread out their kinetic energy with some assumed spatial distribution. An ion releasing its energy at point  $P$  in the solid contributes energy to the surface point  $O$ , that may induce the atoms in  $O$  to break their bonds and either leave the surface or diffuse along it.

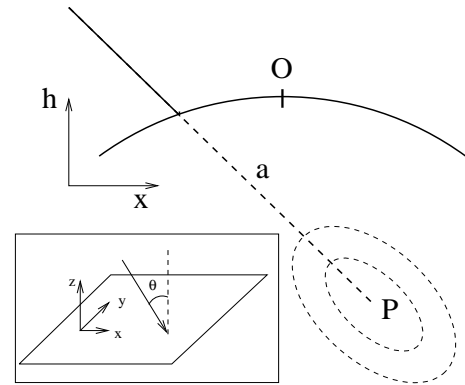


FIG. 1. Following a straight trajectory (solid line) the ion penetrates an average distance  $a$  inside the solid (dotted line) after which it completely spreads out its kinetic energy. The energy decreases with the distance from  $P$ , the dotted curves indicating schematically the equal energy contours. The energy released at point  $P$  contributes to erosion at  $O$ . The inset shows the laboratory coordinate frame: the ion beam forms an angle  $\theta$  with the normal to the *average* surface orientation,  $z$ , and the in-plane direction  $x$  is chosen along the projection of the ion beam.

Following [9,10], we consider that the average energy deposited at point  $O$  due to the ion arriving at  $P$  follows the Gaussian distribution

$$E(\mathbf{r}') = \frac{\epsilon}{(2\pi)^{3/2}\sigma\mu^2} \exp\left\{-\frac{z'^2}{2\sigma^2} - \frac{x'^2 + y'^2}{2\mu^2}\right\}. \quad (1)$$

In (1)  $z'$  is the distance measured along the ion trajectory,  $x'$ ,  $y'$  are measured in the plane perpendicular to it;  $\epsilon$  denotes the kinetic energy of the ion and  $\sigma$  and  $\mu$  are the widths of the distribution in directions parallel and perpendicular to the incoming beam, respectively. However, the sample is subject to an uniform flux  $J$  of bombarding ions. A large number of ions penetrate the solid at different points simultaneously and the velocity of erosion at  $O$  depends on the total power  $\mathcal{E}_O$  contributed by all the ions deposited within the range  $\mathcal{R}$  of the distribution (1), such that

$$v = p \int_{\mathcal{R}} d\mathbf{r} \Phi(\mathbf{r}) E(\mathbf{r}), \quad (2)$$

where  $\Phi(\mathbf{r})$  corrects for the local slope dependence of the uniform flux  $J$  and  $p$  is a proportionality constant between power deposition and the erosion rate [9]. The calculation of  $v$  involves the following assumptions (for more details see Refs. [10,11]): (a) In the *laboratory* coordinate frame  $(x, y, z)$  the surface can be described by a single valued height function  $h(x, y, t)$ , measured from an initial flat configuration which lies in the  $(x, y)$  plane (see Fig. 1); (b) The angle between the ion beam direction and the local normal to the surface is a function of the angle of incidence  $\theta$  and the values of the local slopes  $\partial_x h$  and  $\partial_y h$ , and can be expanded in powers of the latter. Under these conditions, we can expand (2), obtaining the equation of motion [12]

$$\begin{aligned} \frac{\partial h}{\partial t} = & -v_0 + \gamma \frac{\partial h}{\partial x} + \nu_x \frac{\partial^2 h}{\partial x^2} + \nu_y \frac{\partial^2 h}{\partial y^2} + \\ & + \frac{\lambda_x}{2} \left(\frac{\partial h}{\partial x}\right)^2 + \frac{\lambda_y}{2} \left(\frac{\partial h}{\partial y}\right)^2 - D_x^I \frac{\partial^4 h}{\partial x^4} - D_y^I \frac{\partial^4 h}{\partial y^4}. \end{aligned} \quad (3)$$

From (2) we can calculate the expressions for the coefficients appearing in (3) in terms of the physical parameters which characterize the sputtering process. The coefficients  $\nu_x$  and  $\nu_y$  were first calculated by Bradley and Harper [10], while the nonlinear expansion was performed in [11], providing  $\lambda_x$  and  $\lambda_y$ . A fourth order expansion is used to obtain the ion-induced diffusion constants  $D_x^I$  and  $D_y^I$ . To simplify the discussion we restrict ourselves to the symmetric case  $\sigma = \mu$ . Using  $F \equiv (\epsilon J p / \sqrt{2\pi}) \exp(-a_\sigma^2/2 + a_\sigma^2 s^2)$ ,  $s \equiv \sin \theta$ ,  $c \equiv \cos \theta$  and  $a_\sigma \equiv a/\sigma$ , we find for the surface diffusion constants

$$D_x^I = \frac{F a^2}{24 a_\sigma} \{a_\sigma^4 s^4 c^2 + a_\sigma^2 (6c^2 s^2 - 4s^4) + 3c^2 - 12s^2\}, \quad (4)$$

$$D_y^I = \frac{F a^2}{24 a_\sigma} 3c^2. \quad (5)$$

Consistent with symmetry considerations for  $\theta = 0$  we obtain  $D_x^I = D_y^I$ . However, for  $\theta \neq 0$  we find that  $D_x^I \neq D_y^I$ , i.e. the ion-induced surface diffusion is *anisotropic*. Moreover, its sign also depends on the experimental parameters. The consequences of (4) and (5) can be summarized as follows: (a) Independent of the angle of incidence  $D_y^I$  is positive while the sign of the  $D_x^I$  depends on both  $\theta$  and  $a_\sigma$  as shown in Fig. 2.

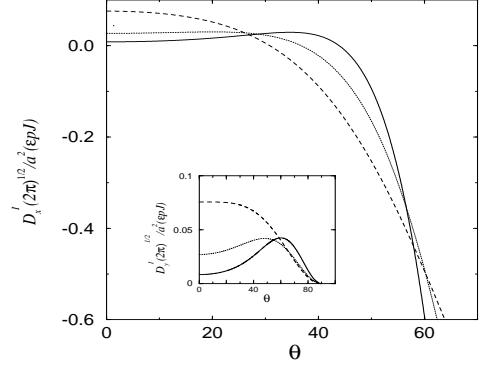


FIG. 2. Ion-induced diffusion constant,  $D_x^I$  and  $D_y^I$  (inset) as a function of the angle of incidence  $\theta$ . In both figures the curves correspond to  $a_\sigma = 1.0$  (dashed line),  $a_\sigma = 1.5$  (dotted line) and  $a_\sigma = 2.0$  (continuous line).

Thus, while for  $\theta = 0$  the ion bombardment enhances the surface diffusion ( $D_x^I > 0$ ), for large  $\theta$  it can suppress diffusion; (b) The fact that  $D_x^I$  can be negative indicates that any simple theory connecting the magnitude of the ion-induced diffusion to the energy transferred by the ions to the surface is incomplete, since it can predict only a positive  $D^I$ . In fact,  $D^I$  is the result of a complex interplay between the local *surface topology* and the energy transferred to the surface; (c) The diffusion constants are proportional to the flux  $J$ , in agreement with the detailed experimental study of Cavaille and Dreschner [7]; (d) It is a standard experimental practice to report the magnitude of the ion-enhanced diffusion using an effective temperature  $T^{eff}$  at which the substrate needs to be heated to obtain the same mobility as with ion bombardment [7,8]. We can calculate  $T^{eff}$  using the relation  $D^I + D_0 \exp(-E_a/k_B T) = D_0 \exp(-E_a/k_B T^{eff})$ , that has two important consequences. First, the anisotropic diffusion constant translates into an anisotropic  $T^{eff}$ , i.e. we have  $T_x^{eff} \neq T_y^{eff}$ . The experimental methods used to estimate  $T^{eff}$  could not distinguish  $T_x^{eff}$  and  $T_y^{eff}$  [7,8]. However, current observational techniques should be able to detect the difference between the two directions. Second, while it is generally believed that ion bombardment can only raise the effective temperature since it transfers energy to the surface, the negative  $D^I$  indicates that

along the  $x$  direction one could have  $T_{eff} < T$ . (e) Finally, the results (4)-(5) are based on Sigmund's theory of sputtering [9] that describes sputtering in the linear cascade regime. The energy range when this approach is applicable lies between 0.5 KeV and 1 MeV, the precise lower and upper limits being material dependent. Thus, we do not expect (4)-(5) to apply to low energy (few eV) ion-enhanced epitaxy.

*Ripple formation*— Sputtering may lead to the development of a ripple morphology on the surface [13]. The origin of the ripple formation is an ion-induced instability: valleys are eroded faster than crests, expressed by negative  $\nu_x$  and  $\nu_y$  coefficients in (3) [10]. At short wavelength this instability is balanced by surface diffusion. A linear stability analysis predicts that the observable ripple wavelength is determined by the most unstable mode, and has the wavelength  $\ell = 2\pi\sqrt{D/|\nu|}$ , where  $\nu$  is the largest in absolute value of the negative surface tension coefficients. Accordingly, the wave vector of the ripples is parallel to the  $x$  axis for small  $\theta$  and perpendicular to it for large  $\theta$  [10]. The large length scale behavior is described by the noisy anisotropic Kuramoto-Sivashinsky equation [11,14], leading to roughening [15] or the development of coarsening ripple domains [16].

*Quantitative comparison with experiments*— At finite temperature the total diffusion constant given by  $D = D^I + D_T$ . As  $T$  decreases there is a critical temperature,  $T_c$ , at which  $D^I = D_T$ , so that for  $T < T_c$  the diffusion is dominated by its ion-induced component, which is independent of temperature, in agreement with the experimental results of MacLaren *et al.* [5]. Unfortunately, for most materials the quantities entering in  $F$ ,  $a_\sigma$  and  $D_0$  are either unknown, or only their order of magnitude can be estimated. However, using the expression for  $\ell$  we can express  $T_c$  in terms of measurable quantities free of these constants

$$T_c = \frac{T_0}{1 - (2k_B T_0 / E_a) \ln(\ell_{Ion} / \ell_{T_0})} \quad (6)$$

where  $\ell_{T_0}$  is the experimentally measured ripple wavelength at any temperature  $T_0 > T_c$ ;  $\ell_{Ion}$  is the ripple wavelength in the low temperature regime,  $T < T_c$ , where ion induced diffusion dominates, and therefore  $\ell_{Ion}$  is independent of  $T$ ;  $E_a$  is provided by the slope of  $\ln(\ell)$  versus  $1/T$  in the high temperature regime ( $T \gg T_c$ ). Consequently, *all* quantities in (6) can be obtained from a plot of the ripple wavelength as a function of temperature, so that (6) gives  $T_c$  *without any free parameters*. Such a plot is provided by MacLaren *et al.* [5], leading to  $E_a = 0.51\text{eV}$ ,  $\ell_{Ion} = 0.8\mu\text{m}$ . Using  $\ell_{T_0} = 2\mu\text{m}$  for  $T = 368\text{K}$  [5], we obtain  $T_c = 57^\circ\text{C}$ , which is in good agreement with the experiments, that provide  $T_c$  between 45 and 60°C [5].

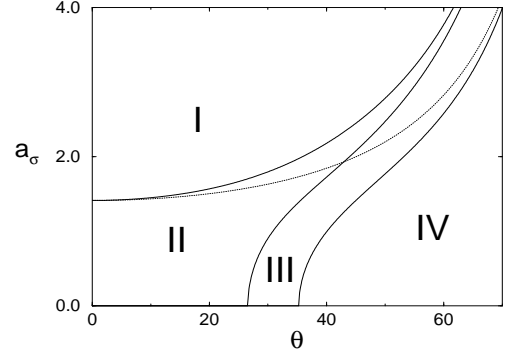


FIG. 3. Phase diagram for the isotropic case  $\sigma = \mu = 1$ . Region I:  $\nu_x < 0$ ,  $\nu_y < 0$ ,  $D_x^I > 0$ ,  $D_y^I > 0$  and  $\ell_x > \ell_y$ ; Region II:  $\nu_x < 0$ ,  $\nu_y < 0$ ,  $D_x^I > 0$ ,  $D_y^I > 0$ , and  $\ell_x < \ell_y$ ; Region III:  $\nu_x < 0$ ,  $\nu_y < 0$ ,  $D_x^I < 0$  and  $D_y^I > 0$ ; Region IV:  $\nu_x > 0$ ,  $\nu_y < 0$ ,  $D_x^I < 0$  and  $D_y^I > 0$ . Note that the phase diagram is independent of the precise values of  $J, p$ , while the  $\epsilon$  dependence is contained in  $a_\sigma$ .

*Morphological phase diagram*— The detailed morphological phase diagram is rather complex if the diffusion is not thermally activated but ion-induced. At low temperatures, when  $D_T$  is negligible compared to  $D^I$ , the ripple wavelengths are  $\ell_x^I = 2\pi\sqrt{D_x^I/|\nu_x|}$  and  $\ell_y^I = 2\pi\sqrt{D_y^I/|\nu_y|}$ . In the following we discuss the dependence of the surface morphologies on the experimental parameters  $\theta$  and  $a_\sigma$ , based on the phase diagram shown in Fig. 3.

*Region I*— The surface tensions,  $\nu_x$  and  $\nu_y$ , are negative while  $D_x$  and  $D_y$  are positive, consequently we have a superimposed ripple structure along the  $x$  and the  $y$  directions. The experimentally observed ripple wavelength is the smallest of the two, and since  $\ell_x^I > \ell_y^I$ , the ripple wave vector is oriented along the  $x$  direction. The lower boundary of this region separating it from Region II is given by the solution of the  $\ell_x^I = \ell_y^I$  equation.

*Region II*— Here the ripple wave vector is oriented along the  $y$  direction, since  $\ell_x^I < \ell_y^I$ . This region is bounded below by the  $D_x^I = 0$  line. At large length scales in I and II one expects kinetic roughening described by the KPZ equation [11,18,17].

*Region III*— In this region  $D_x^I$  is negative, while the sign of all other coefficients are the same as in I and II. Since both surface tension and surface diffusion are destabilizing along  $x$ , every mode is unstable and one expects that the KPZ nonlinearity cannot turn on the KS stabilization [11], the system being unstable at large length scales as well. This instability is expected to lead to exponential roughening. The lower boundary of this region is given by the  $\nu_x = 0$  line.

*Region IV*— Here we have  $\nu_x > 0$ ,  $\nu_y < 0$ ,  $D_{xx}^I < 0$  and  $D_{yy}^I > 0$ , i.e. one expects the surface to be periodically modulated in the  $y$  direction, leading to a ripple structure oriented along the  $x$  direction. In the  $x$  di-

rection we have a reversal of the instability: the short length scale instability generated by the negative  $D_x^I$  is stabilized by the positive surface tension  $\nu_x$ . Thus, there is no ripple structure along the  $y$  direction. Regarding the large length scale behavior, along the  $x$  direction the surface diffusion term is irrelevant compared to the surface tension, thus one expects KPZ scaling. However, along the  $y$  direction the KS mechanism is expected to act, renormalizing the negative  $\nu_y$  to positive values for length scales larger than  $\ell_y^I$ , leading to a large wavelength KPZ behavior.

If thermal and ion-induced diffusion coexist, the ripple wavelengths are given by  $\ell_x = 2\pi[(D_T + D_x^I)/|\nu_x|]^{1/2}$  and  $\ell_y = 2\pi[(D_T + D_y^I)/|\nu_y|]^{1/2}$ . The phase diagram for intermediate temperatures can be calculated using the total  $D$ . In particular for high  $T$ , when  $D_T \gg D_x^I$  and  $D_T \gg D_y^I$ , the phase diagram converges to the one obtained in Ref. [11], the ripple orientation being controlled by the  $\nu_x = \nu_y$  line (dotted in Fig. 3). Thus, with increasing  $D_T$  the phase boundary between the regions I and II converges to the  $\nu_x = \nu_y$  line and the  $D_x = 0$  boundary separating the regions II and III shifts downwards, eventually disappearing. However, in the intermediate regions new phases with coarsening ripple domains [16] appear as the  $D_x^I$  and the  $\nu_x = 0$  lines cross each other.

While we limited our discussion to the effect of the ion-induced diffusion on the surface morphology, the results (4)-(5) can be used to investigate other phenomena as well, such as island nucleation. The experimental verification of the above results would constitute an important step to elucidate the mechanism responsible for ion-induced diffusion, with potential applications to ion-enhanced epitaxy.

We would like to acknowledge discussions and comments by R. Cuerno. This research was partially supported by the University of Notre Dame Faculty Research Program.

- 
- [1] *Sputtering by Particle Bombardment*, R. Behrisch, ed. (Springer-Verlag, Heidelberg 1981, 1983), Vols. I, II, III; *Handbook of Ion Beam Processing Technology*, J.J. Cuomo, S.M. Rossnagel, and H.R. Kaufman, eds. (Noyes Publications, Park Ridge 1992); *Ion Beam Assisted Film Growth*, T. Itoh ed. (Elsevier, Amsterdam, 1989).
- [2] C. Herring, J. Appl. Phys. **21**, 301 (1950); W. W. Mullins, J. Appl. Phys. **28**, 333 (1957); in the context of stochastic models see D. E. Wolf and J. Villain, Eu-

- rophys. Lett. **13**, 389 (1990); S. Das Sarma and P. I. Tamborenea, Phys. Rev. Lett. **66**, 325 (1991).
- [3] V.O. Babaev, Ju.V. Bukov, and M.B. Guseva, Thin Solid Films **38**, 1 (1976).
- [4] M. Marinov, Thin Solid Films **46**, 267 (1977).
- [5] S.W. MacLaren, J.E. Baker, N.L. Finnegan, and C.M. Loxton, J. Vac. Sci. Technol. A **10**, 468 (1992).
- [6] S.A. Barnett, H.F. Winters, and J.E. Greene, Surf. Sci. **181**, Zh.I. Dranova and I.M. Mikhailovskii, Soviet Physics-Solid State **12**, 104 (1970); E. Chason *et al.*, Appl. Phys. Lett. **57**, 1793 (1990); E. Kay and S. M. Rossnagel, in *Handbook of Ion Beam Processing Technology*, in Ref. [1]. (1987).
- [7] J.Y. Cavaille and M. Drechsler, Surf. Sci. **75**, 342 (1978).
- [8] S.M. Rossnagel, R.S. Robinson, and H.R. Kaufman, Surf. Sci. **123**, 89 (1982).
- [9] P. Sigmund, Phys. Rev. **184**, 383 (1969); J. Mat. Sci. **8**, 1545 (1973).
- [10] R. M. Bradley and J. M. E. Harper, J. Vac. Sci. Technol. A **6**, 2390 (1988).
- [11] R. Cuerno and A.-L. Barabási, Phys. Rev. Lett. **74**, 4746 (1995); A.-L. Barabási and R. Cuerno, [Proc. MRS Fall Meeting, Vol. 407, Boston 1995] (MRS, Pittsburgh, 1995).
- [12] In the expansion of (1) additional second, third and fourth order (linear and nonlinear) terms are obtained on the rhs of Eqn. (3) that are not shown here, since they are irrelevant regarding the discussed phenomena (see also Ref. [11]).
- [13] E. Chason *et al.*, Phys. Rev. Lett. **72**, 3040 (1994); T. M. Mayer, E. Chason and A. J. Howard, J. Appl. Phys. **76**, 1633 (1994); G. Carter, B. Navinšek and J. L. Whitton in Vol. II of Ref. [1], p. 231.
- [14] Y. Kuramoto and T. Tsuzuki, Prog. Theor. Phys. **55**, 356 (1977); G. I. Sivashinsky, Acta Astronaut. **6**, 569 (1979).
- [15] E. A. Eklund *et al.*, Phys. Rev. Lett. **67**, 1759 (1991); Surf. Sci. **285**, 157 (1993); J. Krim *et al.*, Phys. Rev. Lett. **70**, 57 (1993); H.-N. Yang, G.-C. Wang, and T.-M. Lu, Phys. Rev. **B 50**, 7635 (1994).
- [16] M. Rost, and J. Krug, Phys. Rev. Lett. **75**, 3894 (1995).
- [17] M. Kardar, G. Parisi and Y.-C. Zhang, Phys. Rev. Lett. **56**, 889 (1986).
- [18] *Dynamics of Fractal Surfaces*, F. Family and T. Vicsek, eds. (World Scientific, Singapore, 1991); W.M. Tong, and R.S. Williams, Annu. Rev. Phys. Chem. **45**, 405 (1994); J. Kertész and T. Vicsek, in *Fractals in Science*, edited by A. Bunde and S. Havlin (Springer-Verlag, Heidelberg, 1994); J. Krug and H. Spohn, in *Solids Far From Equilibrium: Growth, Morphology and Defects*, edited by C. Godrèche (Cambridge Univ. Press, Cambridge, England, 1991); A.-L. Barabási and H. E. Stanley, *Fractal Concepts in Surface Growth* (Cambridge University Press, Cambridge, 1995).